A MUMFORD-SHAH LEVEL-SET APPROACH FOR GEOMETRIC IMAGE REGISTRATION

MARC DROSKE* AND WOLFGANG RING♯

Abstract. A new, fully automated method for non-rigid registration of multi-modal images is presented. Due to the large interdependance of segmentation and registration, the approach is based on simultaneous segmentation and edge-alignment. The two processes are directly coupled and thus benefits from using complementary information of the entire underlying dataset. It is formulated as a variational joint free discontinuity problem in the Mumford-Shah framework, with respect to a geometric variable describing the contour set and a functional variable which represents the underlying deformation. The contour set is represented by a level-set function. We derive a regularized gradient flow and describe an efficient numerical method using and Finite Element discretization and multigrid techniques. Finally, we illustrate the method in several applications, such as multi-modal intra-patient registration and reconstruction by registration to a reference object.

1. Introduction

The registration, i. e. the spatial alignment of images is a fundamental problem in image processing. Given a pair of images, a template and a reference image, it aims at finding a suitable transformation of the template image, such that it is as similar as possible to the reference image. The requirement to register two data sets occurs in various applications, especially in medicine, geophysics and computer vision. In the last two decades there has been a steep increase in variety as well as quality of modern (especially medical) imaging technology, thus making a large amount of information, either anatomical (e. g. computed tomography (CT), magnetic resonance imaging (MRI), ultrasound, densiometry computer tomography (DXA)) or functional(e. g. functional MRI, positron emission tomography (PET,SPECT)) available for clinical routine. The spatial correspondence of the different images is of significant benefit to the clinician, since the whole spectrum of sensoring technology provides images with complementary information. For instance, in radiotherapy treatment planning, CT is mainly used, while MRI allows a detailed analysis of the tumor tissue.

On the other hand, the transformation (the spacial correspondence of like points) itself can provide additional information. A transformation between subsequent images obtained at a very low temporal resolution can give insight into growth

Date: November 14, 2005.

1991 *Mathematics Subject Classification.* 49F22.

Key words and phrases. Image registration, active contours, level-set method, shape sensitivity analysis, Mumford-Shah functional.

This collaboration was initiated during the participation of the authors at the long term program "Inverse Problems: Computational Methods and Emerging Applications", September 8 - December 12, 2003 at the Institute for Pure and Applied Mathematics, University of California Los Angeles.

This work is partially supported by the Deutsche Forschungsgemeinschaft (DFG) as part of the priority program "Mathematical methods for time series analysis and digital image processing" (SPP 1114).

processes of characteristic objects found in the image. In this context, the variability of subsequent image acquisitions may be substantial, leading to difficulties for differential approaches as e.g. *optical-flow* estimation. Furthermore, the resulting transformation of a registration to a healthy reference dataset may be useful to measure the extent of the pathology of the individual patient. Scale-space and multi-resolution methods have become a widely used methodology for variational registration approaches [21, 35, 36, 47] and a wide range of regularization techniques and similarity measures are known [26, 39, 44, 46, 48, 62].

Depending on the nature of the underlying input data, the *richness* of the space of possible deformation plays an important rôle. If it is *a-priori* known that the given multichannel data can be registered by a rigid transformation, the unknowns within the representation are only the offset and angle of the rigid transformation. In that case, regularity of the deformation is automatically guaranteed by the choice of the space of admissible functions. In many applications, especially interpatient-registration, it is, however, of crucial importance to choose a space of higher resolution in order to be able resolve local variations in fine geometrical details, offering the possibility of a comprehensive analysis of the deformation field. In case of medical time series analysis of a single patient, growth processes of pathological objects such as tumors are of significant interest for diagnosis as well as surgery-planning. In what follows the computational resolution of the discretization of the deformation will be the same as the resolution of the input images, allowing a registration of details of pixel accuracy. However, we want to point out, that different (coarser) spaces of deformations may be incorporated in a straightforward manner.

The paper is organized as follows. In Section 2 the approach of coupling registration to segmentation by the Mumford-Shah functional is formulated as a variational, joint free discontinuity problem. Furthermore different regularization techniques are discussed. In Section 3 we present the necessary shape sensitivity analysis by using the conceptional framework of shape derivatives. This eventually leads to the formulation of a gradient flow equation for the given cost functional. To stabilize the shape gradient method, we propose regularizations for both, the descent directions for the shape variable, and the functional variable. This is done in Section 4. In Section 5 we will describe the actual algorithm to compute stationary points of the variational formulation proposed in Section 2. Composite Finite Elements (CFEs) as introduced by Sauter and Hackbusch [34] (see also [56, 61]) provide an elegant approach for the discretization of PDE's on complicated domains and, further, allow to circumvent numerical difficulties for problems with discontinuous coefficients, especially in the context of multigrid solvers. Since we will treat the variational formulation as a shape optimization problem with contours evolving according to the shape analysis, and — as it turns out — certain elliptic PDE's have to be solved in every gradient step, we chose the CFE framework to incorporate efficient multigrid solvers. This is described briefly in Section 6. Finally, computational results are presented in 7 and a final conclusion is drawn in Section 8.

2. Problem Formulation

The aim of this paper to find a registration between two given two- or three-dimensional images based on a matching of the edges in the images. In their pioneering paper, Mumford and Shah [50] introduced the following energy functional:

$$E_{\mathrm{MS}}(u,\Gamma) = \mu \int_{\Omega} (u-u_d)^2 \,\mathrm{d}\mathbf{x} + \int_{\Omega\setminus\Gamma} |\nabla u|^2 \,\mathrm{d}\mathbf{x} + \alpha \mathcal{H}^{n-1}(\Gamma) \tag{2.1}$$

where u_d is a given image defined on an open bounded set $\Omega \subset \mathbb{R}^n$ and u is aimed to be a approximation of u_d which should be smooth on $\Omega \setminus \Gamma$, where Γ is the set of potential edges (i.e. subsets of Hausdorff dimension $n-1$ located at singularities of the given image). Here $\mathcal{H}^{n-1}$ denotes the $n-1$ dimensional Hausdorff measure and μ, α are positive weights, which control the balance between data fit, regularization of the reconstruction u on $\Omega \setminus \Gamma$, and the length of the contour Γ respectively. Existence theory for (2.1) was established after De Giorgi, Carriero and Leaci [27] proposed to consider the minimization of an equivalent energy depending on u only.In this formulation, the energy given by an integral over the entire domain Ω and Γ is represented by S_u the complement set of Lebesgue points of u, i. e. the measure theoretic discontinuity set of u. It can be proved (cf. Ambrosio, Fusco, Pallara [1, 8]) using compactness of $SBV(\Omega)$ and lower-semicontinuity theorems, that — under mild conditions — there exists a solution $u \in SBV(\Omega)$ with $\mathcal{H}^{n-1}(S_u) < \infty$. From the numerical point of view, discretizing the singularity set poses a serious problem. Various approximations E_ϵ of the Mumford-Shah functional have been introduced and Γ-convergence results have been proved (cf. e. g. [2, 3, 6, 55]). Ambrosio and Tortorelli [3], for example, proposed a phase-field type regularization and introduced an auxiliary variable which itself is regularized by an elliptic functional. Here, we refer to Feng and Prohl [32] for the numerical analysis of the phase-field approximation. Bourdin and Chambolle [7] proved Γ-convergence of the discretized finite element schemes.

The Mumford-Shah model has turned out be very versatile and has been extended and applied in various ways [15, 23, 24, 25, 49, 59]. Esedoglu and Shen [30] suggested an inpainting method based on the Mumford-Shah idea. Further modifications have been made concerning the data-fit term in the Mumford-Shah functional, where the simple L^2 distance has been replaced by more elaborate data-fit criteria [].

In this paper we shall use a Mumford-Shah idea for simultaneously finding the singularity sets in two given images and mapping the respective sets (and with them the two images) onto each other. We do not use a reformulation of the Mumford-Shah functional in the sense of De Giorgi, Carriero and Leaci [27]. Instead, we will discretize the discontinuity set Γ directly by a level-set function. For the purpose of segmentation and registration we can confine to simple interface sets, which can be elegantly described and propagated via the level-set approach of Osher and Sethian [53, 54]. Level set methods have been successfully applied in various geometric segmentation models [17, 12, 13, 41, 45, 52, 60]. In [37] Hintermüller and Ring have derived a Newton-Type regularized optimization algorithm for minimizing the Mumford-Shah functional by representing Γ by a level-set function.

In our approach to the segmentation-registration problem, the edge sets in the images are found as minimizers of Mumford-Shah functionals and mapped onto each other by the registration mapping Φ. To be more precise, the edge sets are found in such a way that a level-set encoded contour describes the edge set in the reference image, and, simultaneously, a transformation of the contour by a regular deformation matches the edge set of the template image. This is demonstrated in Figure 2, where only a small part of the edges actually overlap. We emphasize that this viewpoint is different from splitting this process into successively identifying the edge sets first and determining the corresponding deformation which maps these sets onto each other afterwards.

Naturally, the strategy described above would determine the registration map only on the edge set. Therefore, an energy term acting on Φ is added to the Mumford-Shah energy to ensure uniqueness for the registration mapping away from the edge set. As mentioned above, we choose the formulation of the Mumford-Shah

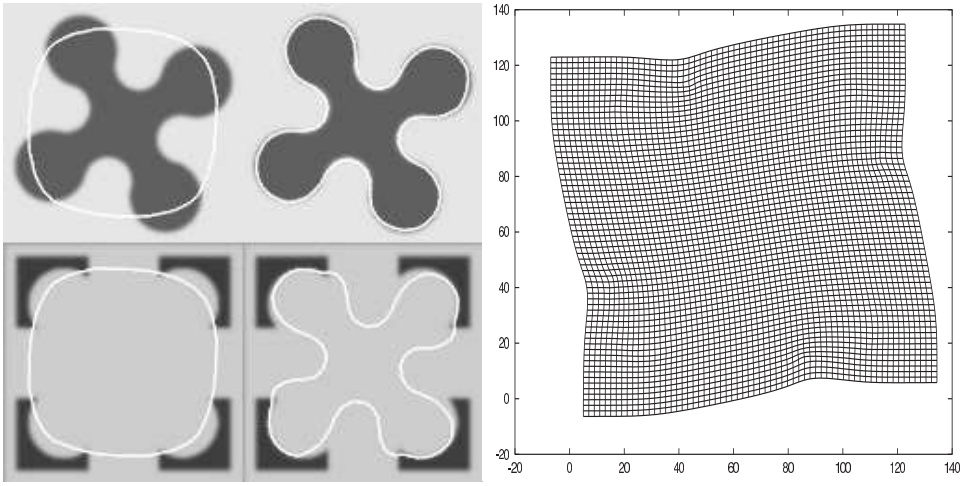

FIGURE 1. Multimodal complementary registration. The two images on the left show the initial contour Γ in the images R and T where the initial deformation is the identity. On the right of the initial images, the resulting contours, coupled by the deformation (right image) are shown after 75 steps of the regularized gradient descent.

energy which is defined for independent geometric and functional variables as e.g. described in [4, Section 4.2.1]. In this formulation, the problem of minimizing the Mumford-Shah functional can be treated as a shape optimization problem and solved numerically using level-set techniques [16, 17, 18, 37]. More precisely, we consider the following functional

$$E_{\mathrm{MS}}(\Gamma,\Phi,R,T) = \frac{1}{2}\int_D |R-R_0|^2\,\mathrm{d}\mathbf{x} + \frac{\mu}{2}\int_{D\setminus\Gamma} |\nabla R|^2\,\mathrm{d}\mathbf{x} + \frac{1}{2}\int_D |T-T_0|^2\,\mathrm{d}\mathbf{x} + \frac{\mu}{2}\int_{D\setminus\Gamma^\Phi} |\nabla T|^2\,\mathrm{d}\mathbf{x} + \alpha\mathcal{H}^{N-1}(\Gamma) \tag{2.2}$$

(the additional regularization term on Φ is omitted for the moment). Here $D \subset \mathbb{R}^N$ is the domain of definition of the images with $N = 2, 3$, the data T_0 and R_0 are the given template images, $\Gamma \subset D$ is (an approximation of) the edge set of the given image R_0 and $\Gamma^\Phi = \Phi(\Gamma)$ is the transformed edge-set Γ under the transformation Φ. Strictly speaking, the term "edge sets of the data images", does not make sense, since the input images only have to be in L^2. When using this term we mean (approximations of) the measure theoretic discontinuity sets of the SBV functions R and T which *approximate* R_0 and T_0 in the Mumford-Shah sense. In the following we make the simplifying assumption that $\Gamma = \partial\Omega$ for an open set Ω with $\overline{\Omega} \subset D$. This assumption is justified if the edge-sets in the data are related to object boundaries as it is usually the case in medical data sets.

Let us point out here, that different approaches can be used to drive the contour Γ towards the significant features of the images. A geodesic active contour model as proposed by Caselles, Kimmel and Sapiro [14], would e.g. lead to a coupled energy of the form

$$E_{\mathrm{ac}}(\Gamma,\Phi) = \int_\Gamma g_R d\mathcal{H}^{n-1} + \nu\int_\Omega g_R\,\mathrm{d}\mathbf{x} + \int_{\Gamma^\Phi} g_T d\mathcal{H}^{n-1} + \nu\int_\Omega g_T\,\mathrm{d}\mathbf{x}, \tag{2.3}$$

where g_R and g_T are suitable edge detectors for the images R and T. A common choice is, for example, $g_I(x) = \frac{1}{1+s|\nabla I|^2}$, $s > 0$ with $I = R$ or $I = T$. The idea of coupling segmentation with registration has also been proposed by Yezzi, Zöllei and Kapur [40].

As already pointed out, the transformation Φ is not uniquely determined by the functional (2.2). Thus, an additional regularization term E_{reg} is necessary. Writing the transformation $\Phi = \mathbf{id} + \mathbf{d}$ with a displacement vector field $\mathbf{d} : D \to \mathbb{R}^2$, we use $\mathbf{d}$ as optimization variable instead of Φ. We set

$$E(\Gamma, \mathbf{d}, R, T) = E_{\text{MS}}(\Gamma, \mathbf{d}, R, T) + \nu E_{\text{reg}}(\mathbf{d}) \tag{2.4}$$

In the following we will use Φ and $\mathbf{d}$ synonymous to denote the transformation.

There is a wide range of different choices of regularizations energies in the literature. Apart from adding a Dirichlet-integral which corresponds to a regularization as proposed by Horn and Schunk in [38] and anisotropic inhomogenous regularizations introduced by Nagel and Enkelmann in [51] – both originally appearing in the *optical-flow* context – linearized elastic regularizations are widely used. In [29] Droske and Rumpf proposed a nonlinear elastic polyconvex regularization energy [19] of the form

$$E_{\text{reg}}(\mathbf{d}) = \int_\Omega \alpha \|\nabla \mathbf{d}\|^p + \beta \|\mathbf{Cof}\, \nabla \mathbf{d}\|^q + \gamma(\det \mathbf{d})\, \mathrm{d}\mathbf{x}, \tag{2.5}$$

where $\gamma(s) \to \infty$ for $s \to 0, \infty$. This approach allows to utilize injectivity techniques for elasticty introduced by Ball [5] in order to ensure that the resulting deformation is a homeomorphism. In the context of aligning feature sets this is particularly important, since we want the transformed contour Γ^Φ to have the same topology as Γ. An extensive discussion of appropriation regularization terms penalizing the departure from rigidity in the context of image registration can be found in Keeling and Ring [42].

At this point of the investigation, the study of different regularization strategies is not our major objective. For the sake of simplicity we will use the Dirichlet integral

$$E_{\text{reg}}(\mathbf{d}) = \|\mathbf{d}\|^2_{\mathbf{H}^1_0(D)} = \int_D \|\nabla \mathbf{d}\|^2\, \mathrm{d}\mathbf{x}, \tag{2.6}$$

as regularization term for the remainder of this paper.

2.1. **The reduced functional.** The functional (2.4) is quadratic in the variables R and T. It is therefore possible to minimize E with respect to R and T for fixed Γ and $\mathbf{d}$ by solving a linear optimality system. With this, we can consider the reduced functional

$$\hat{E}(\Gamma, \mathbf{d}) = E(\Gamma, \mathbf{d}, R(\Gamma), T(\Gamma, \mathbf{d})), \tag{2.7}$$

where $R(\Gamma)$ and $T(\Gamma, \mathbf{d})$ denote the minimizers of (2.4) for fixed Γ and $\mathbf{d}$ with respect to R and T. It is obvious that $R(\Gamma)$ depends only on Γ, whereas $T(\Gamma, \mathbf{d})$ depends also on $\mathbf{d}$ via the domain of integration $D \setminus \Gamma^{\mathbf{d}} = D \setminus \Gamma^{\Phi(\mathbf{d})}$ in the last term in (2.2). If we specify the functional spaces for the variables R and T as $R \in H^1(D \setminus \Gamma)$ and $T \in H^1(D \setminus \Gamma^{\mathbf{d}})$, we find $R(\Gamma)$ and $T(\Gamma, \mathbf{d})$ as solutions to the systems of optimality conditions

$$\begin{aligned} \left\langle \frac{\partial E}{\partial R}, \varphi \right\rangle_{(H^1(D\setminus\Gamma))^*, H^1(D\setminus\Gamma)} &= 0 \text{ for all } \varphi \in H^1(D \setminus \Gamma); \\ \left\langle \frac{\partial E}{\partial T}, \psi \right\rangle_{(H^1(D\setminus\Gamma^{\mathbf{d}}))^*, H^1(D\setminus\Gamma^{\mathbf{d}})} &= 0 \text{ for all } \psi \in H^1(D \setminus \Gamma^{\mathbf{d}}). \end{aligned} \tag{2.8}$$

This yields

$$\mu \int_{D\setminus\Gamma} \langle \nabla R(\Gamma), \nabla \varphi \rangle \,\mathrm{d}\mathbf{x} + \int_{D\setminus\Gamma} R(\Gamma)\,\varphi \,\mathrm{d}\mathbf{x} = \int_{D\setminus\Gamma} R_0\,\varphi \,\mathrm{d}\mathbf{x} \tag{2.9}$$

for all $\varphi \in H^1(D \setminus \Gamma)$ and

$$\mu \int_{D\setminus\Gamma^{\mathbf{d}}} \langle \nabla T(\Gamma,\mathbf{d}), \nabla \psi \rangle \,\mathrm{d}\mathbf{x} + \int_{D\setminus\Gamma^{\mathbf{d}}} T(\Gamma,\mathbf{d})\,\psi \,\mathrm{d}\mathbf{x} = \int_{D\setminus\Gamma^{\mathbf{d}}} T_0\,\psi \,\mathrm{d}\mathbf{x} \tag{2.10}$$

for all $\psi \in H^1(D \setminus \Gamma^{\mathbf{d}})$.

3. Sensitivity Analysis

In this section we derive the expressions for the derivatives $\langle \frac{\partial \hat{E}}{\partial \mathbf{d}}, \boldsymbol{\delta} \rangle$ and $dE\,((\Gamma,\mathbf{d}),F)$. The latter expression denotes the Eulerian derivative of the functional $\hat{E}$ in direction of a perturbation vector field of the form $F\,\mathbf{n}_\Gamma$, where $\mathbf{n}_\Gamma$ is the exterior unit normal vector field to Γ. We assume that $\Gamma = \partial\Omega \subset D$ and we specify the exterior direction with respect to Ω. See [58, 28] for the concepts of classical shape sensitivity analysis, [37, Appendix A.1] and [**?**, 9] for a more level-set based derivation of the classical results. We refer also to [11], where a framework is presented which includes the concept of topological derivative into level-set methods.

3.1. Basic shape derivative formulas.

Let us give a brief overview on the calculus of variations for energies which depend on a geometric variable as e.g. a subdomain Ω, of a fixed domain D or a submanifold Γ of D. For a smooth vectorfield $\vec{V} : D \to \mathbb{R}^n$ with $\overline{\Omega} \subset D$ let us first consider the initial value problem

$$\begin{aligned} X'(t) &= \vec{V}(X(t)) \\ X(0) &= X_0 \end{aligned} \tag{3.1}$$

for $X_0 \in D$. The flow $T_t : \Omega \to \mathbb{R}^n$ (with respect to $\vec{V}$) is then defined as $T_t(x) = X(t)$ where is $X(t)$ is the solution of (3.1) with $X_0 = x$. For a functional $E : \mathcal{E} \to \mathbb{R}$, and a fixed perturbation vectorfield $\vec{V}$, the *Eulerian derivative* is defined by

$$dE(\Gamma;\vec{V}) = \lim_{t\searrow 0} \frac{E(T_t(\Gamma)) - E(\Gamma)}{t} \tag{3.2}$$

provided that the limit exists. Here $\mathcal{E} \subset 2^D$ denotes a suitable set of geometrical variables. The functional E is said to be shape-differentiable at Γ if the limit exists for all $\vec{V} \in B$ and if $dE(\Gamma) \in B'$ i.e. $dE(\Gamma)$ is a bounded linear functional on B, where B is a Banach space of perturbation vector fields. The analogous definitions apply to functions $E(\Omega)$ depending on open sets, not on submanifolds. We will need the following result [58].

Lemma 1. *Let Γ be a $\mathcal{C}^2$-hypersurface, and $f \in H^2_{\mathrm{loc}}(\mathbb{R}^n)$. Then the functional*

$$E(\Gamma) = \int_\Gamma f \,\mathrm{d}\mathcal{H}^{N-1}$$

is shape differentiable for any perturbation $\vec{V} \in \mathcal{C}^1_0(\mathbb{R}^n)$ and the shape derivative is given by

$$E(\Gamma;\vec{V}) = \int_\Gamma \Big(\nabla f \cdot \vec{V} + f\,\mathrm{div}_\Gamma \vec{V} \Big) \,\mathrm{d}\mathcal{H}^{N-1} \tag{3.3}$$

$$= \int_\Gamma \Big(\frac{\partial f}{\partial \mathbf{n}_\Gamma} + f\,\kappa \Big) \vec{V} \cdot n_\Gamma \,\mathrm{d}\mathcal{H}^{N-1} \tag{3.4}$$

where $\mathbf{n}_\Gamma$ denotes the normal to the interface Γ and κ is the additive curvature of Γ.

Definition 1 (material derivative)**.** We consider a family of (sufficiently smooth) open sets $\mathcal{F}$ and we suppose that we are given $f(\Omega) \in B(\Omega)$ for each $\Omega \in \mathcal{F}$, where $B(\Omega)$ is some Banach space of functions on Ω. Let us fix $\Omega_0 \in \mathcal{F}$ and suppose that $\vec{V} \in \mathcal{C}_0^1(\mathbb{R}^n, \mathbb{R}^n)$ be given. We set $\Omega_t = T_t(\Omega_0)$ and assume that $f(\Omega_t) \in B(\Omega_t)$. The limit

$$\dot{f} = \lim_{t \searrow 0} \frac{f(\Omega_t) \circ T_t - f(\Omega_0)}{t}$$

is called the (weak) material derivative, if it exists in the strong (weak) topology on $B(\Omega_0)$.

Definition 2 (shape derivative)**.** If the weak material derivative and the expression $\nabla f(\Omega) \cdot \vec{V}$ exist in $B(\Omega)$, then we set

$$f'(\Omega; \vec{V}) = \dot{f}(\Omega; \vec{V}) - \langle \nabla f(\Omega), \vec{V} \rangle$$

and call it the *shape derivative* of f at Ω in direction V.

In the next section we will also need the following result [58]:

Proposition 1. *Let $f(\Omega)$ be given such the weak L^1-material derivative $\dot{f}(\Omega; \vec{V})$ and the shape derivative $f'(\Omega; \vec{V}) \in L^1(\Omega)$ exist. Then, the functional*

$$E(\Omega) = \int_\Omega f(\Omega, \mathbf{x}) \, \mathrm{d}\mathbf{x}$$

is shape differentiable and the derivative is given by

$$dE(\Omega; \vec{V}) = \int_\Omega f'(\Omega; \vec{V}) \, \mathrm{d}\mathbf{x} + \int_\Gamma f \, \langle \vec{V}, \mathbf{n}_\Gamma \rangle \, \mathrm{d}\mathcal{H}^{N-1}. \tag{3.5}$$

It can be shown (see [58]) that the various concepts of (first) derivatives with respect to a geometric variable depend on the direction of perturbation V only via its projection

$$F = \langle \vec{V}, \mathbf{n}_\Gamma \rangle \tag{3.6}$$

onto the normal direction to Γ. We therefore subsequently write $dE(\Gamma; F)$ instead of $dE(\Gamma; V)$ and likewise for the other types of derivatives.

3.2. **The first variation of the energy.** In the following, we frequently use the coordinate transformation $\mathbf{x} \mapsto \mathbf{y} = \Phi(\mathbf{x}) = \mathbf{x} + \mathbf{d}(\mathbf{x})$ to switch between representations on the transformed and on the original configuration. Finding first variations of the functional (2.4) with respect to the geometry Γ requires differentiation with respect to Γ of functionals $\int_\Omega g \, \mathrm{d}\mathbf{x}$ and $\int_{\Phi(\Omega)} h \, \mathrm{d}\mathbf{x}$, respectively where $\partial\Omega \subset \Gamma$. For integrals of the first type, the results of Section 3 directly apply. Suppose that $T_t(\mathbf{x})$ is a flow map which defines a perturbation of Γ with corresponding vector field $\vec{V}$. Then the perturbation of Γ^Φ is given by the flow map $S_t(\mathbf{y}) = \Phi\big(T_t(\Phi^{-1}(\mathbf{y}))\big)$. The corresponding perturbation vector field has the form $\vec{W}(\mathbf{y}) = \big(\nabla\Phi \cdot \vec{V}\big)(\Phi^{-1}(\mathbf{y}))$. With this, we can apply the results of Section 3 to integrals defined in the transformed configuration. For later use, we recall the following transformation formulas [20]:

$$\mathbf{n}_{\Gamma^\Phi}(\mathbf{y}) = \frac{\mathbf{Cof}\, \nabla\Phi(\mathbf{x}) \cdot \mathbf{n}_\Gamma(\mathbf{x})}{\|\mathbf{Cof}\, \nabla\Phi(\mathbf{x}) \cdot \mathbf{n}_\Gamma(\mathbf{x})\|}, \tag{3.7a}$$

$$F_\Phi := \langle \vec{W}(\mathbf{y}), \mathbf{n}_{\Gamma^\Phi}(\mathbf{y}) \rangle = \frac{\det\nabla\Phi(\mathbf{x})}{\|\mathbf{Cof}\, \nabla\Phi(\mathbf{x}) \cdot \mathbf{n}_\Gamma(\mathbf{x})\|} \langle \vec{V}(\mathbf{x}), \mathbf{n}_\Gamma(\mathbf{x}) \rangle = \frac{\det\nabla\Phi(\mathbf{x})}{\|\mathbf{Cof}\, \nabla\Phi(\mathbf{x}) \cdot \mathbf{n}_\Gamma(\mathbf{x})\|} F, \tag{3.7b}$$

$$\int_{\Gamma^\Phi} g\, d\mathcal{H}^{N-1} = \int_\Gamma g\circ\Phi\ \|\mathbf{Cof}\,\nabla\Phi\cdot\mathbf{n}_\Gamma\|\, d\mathcal{H}^{N-1}, \tag{3.7c}$$

where $\mathbf{Cof}\,A \in \mathbb{R}^{n\times n}$ denotes the cofactor matrix of a matrix $A\in\mathbb{R}^{n\times n}$.

Proposition 1 (see also [58, Section 2.31]) implies that

$$\begin{aligned} d\hat{E}\left((\Gamma,\mathbf{d});F\right) = &\\ &\frac{1}{2}\int_\Gamma \Big(\llbracket|R(\Gamma)-R_0|^2\rrbracket + \mu\llbracket|\nabla_{\mathbf{x}}R(\Gamma)|^2\rrbracket\Big)\, F\, d\mathcal{H}^{N-1}\\ &+\frac{1}{2}\int_{\Gamma^\Phi}\Big(\llbracket|T(\Gamma,\mathbf{d})-T_0|^2\rrbracket\,|+\mu\llbracket|\nabla_{\mathbf{y}}T(\Gamma,\mathbf{d})|^2\rrbracket\Big)\, F_\Phi\, d\mathcal{H}^{N-1}\\ &+\Big\langle\frac{\partial E}{\partial R},R'_F\Big\rangle_{(H^1(D\setminus\Gamma))^*,H^1(D\setminus\Gamma)}+\Big\langle\frac{\partial E}{\partial T},T'_{F_\Phi}\Big\rangle_{(H^1(D\setminus\Gamma^\Phi))^*,H^1(D\setminus\Gamma^\Phi)}\\ &+\int_\Gamma \kappa\, F\, d\mathcal{H}^{N-1}, \end{aligned} \tag{3.8}$$

where $\llbracket\cdot\rrbracket$ denotes magnitudes of jump discontinuities across Γ (from inside to outside) and across Γ_Φ respectively. As above κ is the additive curvature of Γ, R'_F and T'_{F^Φ} are the shape derivatives of R and T in direction to the perturbation given by F and F_Φ respectively. It can be shown (using the techniques described in [58, Sec. 3.2 and 2.29]) that R'_F is solution to the inhomogeneous Neumann-type boundary value problems

$$\int_{\tilde\Omega}\left(\mu\langle\nabla R'_F,\nabla\varphi\rangle + R'_F\,\varphi\right)\mathrm{d}\mathbf{x} = -\int_{\partial\tilde\Omega}\left(\mu\langle\nabla_\Gamma R_F,\nabla_\Gamma\varphi\rangle+(R_F-R_0)\,\varphi\right)F\,d\mathcal{H}^{N-1}$$

on each connected component $\tilde\Omega$ of $D\setminus\Gamma$ and for all $\varphi\in H^1(\tilde\Omega)$. An elliptic regularity result then shows that the solution $R'_F|_{\tilde\Omega}\in H^1(\tilde\Omega)$ for each connected component $\tilde\Omega$ of $D\setminus\Gamma$ and hence $R'_F\in H^1(D\setminus\Gamma)$. Analogously we obtain $T'_{F_\Phi}\in H^1(D\setminus\Gamma^\Phi)$. Here we need to assume that the transformation Φ is sufficiently smooth. Consequently, we can use R'_F and T'_{F_Φ} as test functions in (2.8) to conclude that the last two terms in (3.8) vanish. Transforming all expressions in (3.8) onto the undeformed configuration (using (3.7)) and replacing Φ by $\mathbf{id}+\mathbf{d}$ yields

$$\begin{aligned} d\hat{E}\left((\Gamma,\mathbf{d});F\right) =&\frac{1}{2}\int_\Gamma\left(\llbracket|R(\Gamma)-R_0|^2\rrbracket+\mu\llbracket|\nabla R(\Gamma)|^2\rrbracket\right)\,F\,d\mathcal{H}^{N-1}\\ &+\frac{1}{2}\int_\Gamma\Big(\big\llbracket|T(\Gamma,\mathbf{d})-T_0|^2\circ(\mathbf{id}+\mathbf{d})\big\rrbracket+\\ &\qquad\mu\,\big\llbracket|\nabla T(\Gamma,\mathbf{d})|^2\circ(\mathbf{id}+\mathbf{d})\big\rrbracket\Big)\,|\det(I+\nabla\mathbf{d})|\,F\,d\mathcal{H}^{N-1}\\ &+\alpha\int_\Gamma\kappa\,F\,d\mathcal{H}^{N-1}. \end{aligned} \tag{3.9}$$

We now consider variation with respect to the displacement $\mathbf{d}$. The cost functional depends on $\mathbf{d}$ via the domain of integration $D\setminus\Gamma^{\mathbf{d}}$ and implicitly via $T(\Gamma,\mathbf{d})$. The perturbation of the geometry has the form $\Gamma^{\mathbf{d}+t\,\boldsymbol{\delta}}=\Gamma^{\mathbf{d}}+t\,\boldsymbol{\delta}(\Gamma)=\Gamma^{\mathbf{d}}+t\left(\boldsymbol{\delta}\circ(\mathbf{id}+\mathbf{d})^{-1}(\Gamma^{\mathbf{d}})\right)$. It can be shown [28, Chapt. 7] that this perturbation is equivalent to a perturbation of $\Gamma^{\mathbf{d}}$ with the velocity vector field $\boldsymbol{\delta}\circ(\mathbf{id}+\mathbf{d})^{-1}$.

We can therefore apply the results in Section 3 to obtain

$$\begin{aligned}\Big\langle \frac{\partial \hat{E}}{\partial \mathbf{d}}, \boldsymbol{\delta} \Big\rangle &= \Big\langle \frac{\partial E}{\partial T}, T'\big(\Gamma^{\mathbf{d}}, \boldsymbol{\delta} \circ (\mathbf{id}+\mathbf{d})^{-1}\big) \Big\rangle_{(H^1(D\setminus\Gamma^{\mathbf{d}}))^*, H^1(D\setminus\Gamma^{\mathbf{d}})} \\ &+ \frac{1}{2}\int_{\Gamma^{\mathbf{d}}} \left([\![|T(\Gamma,\mathbf{d}) - T_0|^2]\!] + \mu [\![|\nabla T(\Gamma,\mathbf{d})|^2]\!] \right) \langle \boldsymbol{\delta} \circ (\mathbf{id}+\mathbf{d})^{-1}, \mathbf{n}_{\Gamma^{\mathbf{d}}} \rangle \, d\mathcal{H}^{N-1} \\ &+ \nu \Big\langle \frac{\partial E_{\mathrm{reg}}}{\partial \mathbf{d}}, \boldsymbol{\delta} \Big\rangle.\end{aligned}$$

As above we argue that $T'\big(\Gamma^{\mathbf{d}}, \boldsymbol{\delta} \circ (\mathbf{id}+\mathbf{d})^{-1}\big) \in H^1(D \setminus \Gamma^{\mathbf{d}})$ and the first term vanishes due to (2.8). If the regularization term (2.7) is used, the Frèchet derivative of $\hat{E}$ with respect to $\mathbf{d}$ in direction $\boldsymbol{\delta}$ reads as

$$\begin{aligned}&\Big\langle \frac{\partial \hat{E}}{\partial \mathbf{d}}, \boldsymbol{\delta} \Big\rangle = \\ &\frac{1}{2}\int_{\Gamma^{\mathbf{d}}} \left([\![|T(\Gamma,\mathbf{d}) - T_0|^2]\!] + \mu [\![|\nabla T(\Gamma,\mathbf{d})|^2]\!] \right) \langle \boldsymbol{\delta} \circ (\mathbf{id}+\mathbf{d})^{-1}, \mathbf{n}_{\Gamma^{\mathbf{d}}} \rangle \, d\mathcal{H}^{N-1} \\ &\qquad + \nu \int_D \nabla \mathbf{d} : \nabla \boldsymbol{\delta} \, \mathrm{d}\mathbf{x},\end{aligned} \tag{3.10}$$

where ":" stands for the matrix tensor product, i.e. the scalar product corresponding to the Frobenius norm.

We have not yet specified the function space for the displacement field $\mathbf{d}$. The natural choice corresponding the choice of the regularization E_{reg} would be $d \in \mathbf{H}_0^1(D) = H_0^1(D, \mathbb{R}^n)$. For the application of shape sensitivity results, however, we need more regularity for the transformation $\Gamma \mapsto (\mathbf{id}+\mathbf{d})(\Gamma)$. This issue will be discussed later on when we define updates for the displacement $\mathbf{d}$.

4. Choice of a Descent Direction

We now address the question of finding an appropriate descent direction, i.e. a direction $\boldsymbol{\delta}_d \in \mathbf{H}_0^1(D)$ and a scalar function F_d defined on Γ such that

$$\Big\langle \frac{\partial \hat{E}}{\partial \mathbf{d}}, \boldsymbol{\delta}_d \Big\rangle < 0 \quad \text{and} \quad d\hat{E}\left((\Gamma,\mathbf{d}); F_d\right) < 0. \tag{4.1}$$

The descent directions $\boldsymbol{\delta}_d$ and F_d are found by minimizing the linear approximations over the unit sphere of appropriate function spaces in which the admissible directions are chosen. This idea is closely related to the approach chosen in [21, 22], where the descent direction is determined with respect to a regularizing metric. In our case the metric is the scalar product of the adequately chosen Hilbert space. We leave the question of choice of the correct function space for F_d open for the moment and start with finding a descent direction with respect to $\mathbf{d}$. We say that $\boldsymbol{\delta}_d$ is the direction of steepest descent for $\hat{E}$ with respect to $\mathbf{d}$ and the metric induced by the $\mathbf{H}_0^1(D)$-norm iff $\boldsymbol{\delta}_d$ is solution to the constrained optimization problem

$$\min_{\substack{\boldsymbol{\delta} \in \mathbf{H}_0^1(D) \\ \|\boldsymbol{\delta}\|_{\mathbf{H}_0^1(D)}=1}} \Big\langle \frac{\partial \hat{E}}{\partial \mathbf{d}}(\Gamma,\mathbf{d}), \boldsymbol{\delta} \Big\rangle. \tag{4.2}$$

Note that $\left\langle \frac{\partial \hat{E}}{\partial \mathbf{d}}(\Gamma, \mathbf{d}), \cdot \right\rangle$ defines a bounded linear functional on $\mathbf{H}_0^1(D)$ provided that $\mathbf{d}$ is smooth enough. To solve (4.2), we introduce the Lagrange function

$$\begin{aligned}\mathcal{L}_f(\boldsymbol{\delta}, \lambda_f) = &\\ &\frac{1}{2}\int_{\Gamma^{\mathbf{d}}} \left([\![|T(\Gamma, \mathbf{d}) - T_0|^2]\!] + \mu [\![|\nabla T(\Gamma, \mathbf{d})|^2]\!] \right) \langle \boldsymbol{\delta} \circ (\mathbf{id} + \mathbf{d})^{-1}, \mathbf{n}_{\Gamma^{\mathbf{d}}} \rangle \, d\mathcal{H}^{N-1} \\ &\quad + \nu \int_D \nabla \mathbf{d} : \nabla \boldsymbol{\delta} \, \mathrm{d}\mathbf{x} + \lambda_f \left(\int_D |\nabla \boldsymbol{\delta}|^2 \, \mathrm{d}\mathbf{x} - 1 \right).\end{aligned}$$

The optimality system for (4.2) reads as $\frac{\partial \mathcal{L}_f}{\partial \boldsymbol{\delta}}(\boldsymbol{\delta}_d, \lambda_d) = 0$ and $\frac{\partial \mathcal{L}_f}{\partial \lambda_f}(\boldsymbol{\delta}_d, \lambda_d) = 0$. Therefore, the direction of steepest descent $\boldsymbol{\delta}_d$ is found as the solution to

$$\begin{aligned}(4.3)\quad &\int_D \nabla \boldsymbol{\delta}_d : \nabla \boldsymbol{\xi} \, \mathrm{d}\mathbf{x} = -\frac{1}{\lambda_f} \left(\nu \int_D \nabla \mathbf{d} : \nabla \boldsymbol{\xi} \, \mathrm{d}\mathbf{x} \right. \\ &\left. + \frac{1}{2} \int_{\Gamma^{\mathbf{d}}} \left([\![|T(\Gamma, \mathbf{d}) - T_0|^2]\!] + \mu [\![|\nabla T(\Gamma, \mathbf{d})|^2]\!] \right) \langle \boldsymbol{\xi} \circ (\mathbf{id} + \mathbf{d})^{-1}, \mathbf{n}_{\Gamma^{\mathbf{d}}} \rangle \, d\mathcal{H}^{N-1} \right)\end{aligned}$$

for all $\boldsymbol{\xi} \in \mathbf{H}_0^1(D)$, where the multiplier λ_f is chosen such that $\|\boldsymbol{\delta}_d\|_{\mathbf{H}_0^1(D)} = 1$.

Alternatively one might want to allow $\boldsymbol{\delta}_d \in \mathbf{H}^1$ instead of prescribing homogenous Dirichlet conditions, which can be particularly important in case of large translations between the reference and the template image. Then $\boldsymbol{\delta}_d$ is given as solution of

$$\begin{aligned}(4.4)\quad &\int_D \left(\langle \boldsymbol{\delta}_d, \boldsymbol{\xi} \rangle + \nabla \boldsymbol{\delta}_d : \nabla \boldsymbol{\xi} \right) \mathrm{d}\mathbf{x} = -\frac{1}{\lambda_f} \left(\nu \int_D \nabla \mathbf{d} : \nabla \boldsymbol{\xi} \, \mathrm{d}\mathbf{x} \right. \\ &\left. + \frac{1}{2} \int_{\Gamma^{\mathbf{d}}} \left([\![|T(\Gamma, \mathbf{d}) - T_0|^2]\!] + \mu [\![|\nabla T(\Gamma, \mathbf{d})|^2]\!] \right) \langle \boldsymbol{\xi} \circ (\mathbf{id} + \mathbf{d})^{-1}, \mathbf{n}_{\Gamma^{\mathbf{d}}} \rangle \, d\mathcal{H}^{N-1} \right)\end{aligned}$$

for all $\boldsymbol{\xi} \in \mathbf{H}^1(D)$.

Application of the transformation rules (3.7c) and (3.7b) to the surface integral on the right hand side of (4.3) and (4.4) yields

$$\begin{aligned}(4.5)\quad &\frac{1}{2} \int_{\Gamma} \left([\![|T(\Gamma, \mathbf{d}) - T_0|^2]\!] + \mu [\![|\nabla_{\mathbf{y}} T(\Gamma, \mathbf{d})|^2]\!] \circ (\mathbf{id} + \mathbf{d}) \right) \langle \boldsymbol{\xi}, \mathbf{Cof} \, \nabla \mathbf{d} \cdot \mathbf{n}_{\Gamma} \rangle \, d\mathcal{H}^{N-1}\end{aligned}$$

for these terms.

We now make a few comments concerning the regularity of the displacement $\mathbf{d}$. The update $\boldsymbol{\delta}_d$ which solves (4.3) is a function in $\mathbf{H}_0^1(D)$ which — in general — does not possess much additional regularity since the source term is a distribution which is localized on Γ thus introducing a singularity $\boldsymbol{\delta}_d$ along Γ. For the shape sensitivity results above to hold we need that the displacement is smooth in every step. To circumvent this difficulty, we can replace $\boldsymbol{\delta}_d$ by a smooth approximation $\boldsymbol{\delta}_d^{\epsilon}$ for the actual update of the transformation. If the approximation is close enough in the $\mathbf{H}_0^1(D)$-norm the descent property (4.1) will still be satisfied and the theoretical arguments are justified. In the numerical realization it turns out that smoothing of the transformation is not necessary.

To find a descent direction for the geometrical variable Γ, we first have to specify the function space and the corresponding metric for the update direction F_d. By choosing the update direction $\boldsymbol{\delta}_d \in \mathbf{H}_0^1(D)$, the movement of the transformed geometry $\Gamma^{\mathbf{d}} \mapsto \Gamma^{\mathbf{d}+t\boldsymbol{\delta}_d}$ corresponds to a movement in normal direction with speed function given by

$$F_{\boldsymbol{\delta}_d} = \langle \boldsymbol{\delta}_d, \mathbf{n}_{\Gamma^{\mathbf{d}}} \rangle \in H^{\frac{1}{2}}(\Gamma^{\mathbf{d}}).$$

It is therefore natural to choose the descent direction F also with respect to the $H^{\frac{1}{2}}$-norm on Γ. This choice should give a good balance between the descents achieved

by moving the geometrical variable Γ and the functional variable $\mathbf{d}$ respectively. More precisely, we choose the descent direction F_d as solution to the problem

$$\min_{\substack{F\in H^{\frac{1}{2}}(\Gamma)\\ \|F\|_{H^{\frac{1}{2}}(\Gamma)}=1}} dE\big((\Gamma,\mathbf{d}),F\big). \tag{4.6}$$

We introduce again a Lagrange function

$$\mathcal{L}_g(F,\lambda_g) = d\hat{E}\left((\Gamma,\mathbf{d});F\right) + \lambda_g\left(\|F\|^2_{H^{\frac{1}{2}}(\Gamma)} - 1\right).$$

The optimality system for F_d has then the form

$$(F_d,G)_{H^{\frac{1}{2}}(\Gamma)} = -\frac{1}{\lambda_g} d\hat{E}\left((\Gamma,\mathbf{d});G\right) \tag{4.7}$$

for all $G \in H^{\frac{1}{2}}(\Gamma)$. To evaluate the inner product $(\cdot,\cdot)_{H^{\frac{1}{2}}(\Gamma)}$ we consider the boundary value problem

$$\begin{aligned} -\Delta v + v &= 0 \text{ on } \Omega \\ \frac{\partial v}{\partial n}\Big|_\Gamma &= H \in H^{-\frac{1}{2}}(\Gamma). \end{aligned} \tag{4.8}$$

Here $\Omega \subset D$ is chosen such that $\Gamma = \partial\Omega$. In the level-set context below, Ω can be chosen as the set of all point with negative function values of the level-set function. The weak formulation for (4.8) is given by

$$\int_\Omega \left(\langle\nabla v,\nabla\varphi\rangle + v\,\varphi\right) \mathrm{d}\mathbf{x} = \left\langle H,\varphi|_\Gamma\right\rangle_{H^{-\frac{1}{2}}(\Gamma),H^{\frac{1}{2}}(\Gamma)} \tag{4.9}$$

for all $\varphi \in H^1(\Omega)$. We define the Neumann-to-Dirichlet map for the operator $-\Delta + \mathrm{id}$ on Ω as the linear operator $\mathcal{N} : H^{-\frac{1}{2}}(\Gamma) \to H^{\frac{1}{2}}(\Gamma)$ which maps H in (4.8) to the Dirichlet trace $v|_\Gamma$ of the solution to (4.8). It is well known (see [43]) that $\mathcal{N}$ is an isomorphism and that the inner product on $H^{\frac{1}{2}}(\Gamma)$ can be defined as

$$(F,G)_{H^{\frac{1}{2}}(\Gamma)} = \langle\mathcal{N}^{-1}F,G\rangle_{H^{-\frac{1}{2}}(\Gamma),H^{\frac{1}{2}}(\Gamma)}.$$

With this, we can write (4.7) as

$$\langle\mathcal{N}^{-1}F_d,G\rangle_{H^{-\frac{1}{2}}(\Gamma),H^{\frac{1}{2}}(\Gamma)} = -\frac{1}{\lambda_g} d\hat{E}\left((\Gamma,\mathbf{d});G\right)$$

for all $G \in H^{\frac{1}{2}}(\Gamma)$. If we use (3.9), we obtain

(4.10)

$$\begin{aligned} F_d &= -\frac{1}{\lambda_g}\mathcal{N}F_g \text{ with} \\ F_g &= \frac{1}{2}\Big(\llbracket|R(\Gamma)-R_0|^2\rrbracket + \mu\llbracket|\nabla R(\Gamma)|^2\rrbracket \\ &\quad + \left(\llbracket|T(\Gamma,\mathbf{d})-T_0|^2\circ(\mathbf{id}+\mathbf{d})\rrbracket + \mu\llbracket|\nabla T(\Gamma,\mathbf{d})|^2\circ(\mathbf{id}+\mathbf{d})\rrbracket\right)|\det(I+\nabla\mathbf{d})|\Big) \\ &\quad + \alpha\kappa \end{aligned}$$

on Γ.

5. Description of the Algorithm

Let us now assemble all the discussed main building blocks into a regularized shape gradient descent algorithm within the level-set framework:

Step 1: Choose an initial level-set function u_0, choose an initial transformation $\mathbf{d}_0$. Set $u_c = u_0$, $\mathbf{d}_c = \mathbf{d}_0$.

Step 2: For the current level-set function u_c set $\Omega = \{\mathbf{x} \in D : u_c(\mathbf{x}) < 0\}$, $\Gamma = \{\mathbf{x} \in D : u_c(\mathbf{x}) = 0\}$. Solve the equations (2.9) and (2.10) for R and T respectively for the current Γ and $\mathbf{d}_c$.

Step 3: Evaluate the expression F_g in (4.10).

Step 4: Solve the elliptic equation (4.8) with Neumann data given by F_g. Evaluate the Dirichlet trace to get F_d on Γ.

Step 5: Extend F_d to a function F_d^{ext} which is defined on a narrow band around Γ.

Step 6: Solve (4.3) for $\boldsymbol{\delta}_d$.

Step 7: Solve the level-set equation

$$u_t + F_d^{\text{ext}} |\nabla u| = 0 \quad \text{with } u(\cdot, 0) = u_c$$

Set the new $u_c = u(\cdot, \tau)$. Set $\mathbf{d}_c = \mathbf{d}_c + \tau \boldsymbol{\delta}_d$. Choose the step-size τ according to a line search procedure.

Step 8: Stopping criterion. Else go to Step 2.

The finite element approximations of the functions R and T and the axilliary variable v in (4.9) on the irregular domains $D \setminus \Gamma$, $D \setminus \Gamma^{\mathbf{d}}$ and Ω are done using composite finite elements (c.f. [34]). The transformation vector field $\mathbf{d}$ is discretized using standard finite elements.

5.1. **Step 2.** Equations (2.9) and (2.10) are solved using a composite finite elements for the solution of the second order elliptic equations on the variable and irregular domains $D \setminus \Gamma$ and $D \setminus \Gamma^{\mathbf{d}}$. The composite finite element code takes as input the function values of a level-set function, which defines the variable geometry, on a rectangular grid. For $D \setminus \Gamma$ the level-set function is given by u_c. For the transformed geometry $D \setminus \Gamma^{\mathbf{d}}$ a level-set function is given by $u_c^{\mathbf{d}} = u_c \circ (\mathbf{id} + \mathbf{d})^{-1}$. We introduce a triangulation $\mathcal{T}$ on D and approximate $\mathbf{d}$ by a piecewise affine transformation on $\mathcal{T}$.

5.2. **Step 3.** The data F_g are processed further in Step 4 as Neumann boundary data in (4.8). It follows from (4.9) that the data are used in the form $\int_\Gamma F_g \, \varphi_n \, d\mathcal{H}^{N-1}$, for all finite element basis functions φ_n. Hence, it is useful to determine the values of F_g on the intersection points of the rectangular finite element grid with Γ.

In F_g the jumps $R_i - R_e$ and $\nabla R_i - \nabla R_e$ occur, where R_i (interior) is the solution to (2.9) on Ω and R_e (exterior) is the solution to (2.9) on $D \setminus \overline{\Omega}$. We get the function values for R_i and R_e at the intersection points in a straight forward way from the respective finite element representations.

5.3. **Step 4.** In order to calculate F_d in (4.10), we solve

$$(\nabla \phi_i^{CFE}, \nabla \phi_j^{CFE})_{L^2(\Omega_1)} \bar{F}_{d,i} + (\phi_i^{CFE}, \phi_j^{CFE})_{L^2(\Omega_1)} \bar{F}_{d,i} = -\frac{1}{\lambda_g} (F_g, \phi_i)_{L^2(\partial\Omega_1)},$$

where ϕ_i^{CFE} denote the basis functions of the finite elements space (cf. Section 6), and $\bar{F}_{d,i}$ denotes the i-th component of the vector $\bar{F}_d$, i.e. the coefficient vector of F_d with respect to the chosen basis.

5.4. **Step 5.** We now extend F_d given form the discrete contour Γ_h to a function F_d^{ext} defined on a neighborhood of Γ_h by solving the following transport equation:

$$\langle \nabla F_d^{\text{ext}}, \nabla d_\Gamma \rangle = 0 \quad \text{on} \quad \Omega \qquad \text{and} \qquad F_d^{\text{ext}} = F_d \quad \text{on} \quad \Gamma. \tag{5.1}$$

Here d_Γ denotes signed the distance function to Γ. Note, that d_Γ and F_d^{ext} can be computed simultaneously by a modified fast marching method for solving the eikonal equation $|\nabla d| = 1$ (cf. [52, 57] for a comprehensive description of the algorithm).

5.5. **Step 7.** The discretization of the level-set equation

$$\partial_t u + F_d^{\text{ext}} |\nabla u| = 0 \quad \text{on} \quad \Omega \tag{5.2}$$

is carried out using an explicit upwind scheme. In our computations we have applied a third-order accurate ENO-scheme (cf. [52]).

6. Composite Finite Elements and Multigrid

In this section we will briefly describe the spatial descretization of the H^1 function spaces on Ω_i, which are divided by the contour Γ i.e. the zero level-set of u. Furthermore we outline a multigrid method for the solution of (2.9), (2.10), (4.3) and (4.9). We use Composite Finite Elements introduced by Hackbusch and Sauter [34]. Instead of resolving the Ω_i by a retriangulation or local adaptive refinement, we confine ourselves to a uniform quadrilateral resp. hexahedral grid $\mathcal{T}$ and define the triangulations $\mathcal{T}_i$ by the following overlap-condition:

$$\Omega_i \subseteq \overline{\bigcup_{T \in \mathcal{T}_i} T} \quad \text{with } T \in \mathcal{T}_i \iff T \in \mathcal{T}, \quad T \cap \Omega_i \neq \emptyset. \tag{6.1}$$

Let us denote by $V_h(\Omega_{\mathcal{T}})$ the usual Finite Element space given by the condition that for $U \in V_h(\Omega_{\mathcal{T}})$, $U\big|_T$ is a multilinear function for each $T \in \mathcal{T}$. The corresponding Composite Finite Element space is then given by the restriction of the functions in $V_h(\Omega_{\mathcal{T}_i})$ to the domain Ω_i, i. e.

$$V_h^{CFE}(\Omega_{\mathcal{T}_i}) := \{U|_{\Omega_i} \,|\, U \in V_h(\Omega_{\mathcal{T}_i})\}. \tag{6.2}$$

Hence, a basis $(\varphi_i^{CFE})_i$ of V_h^{CFE} is given by $\varphi_i^{CFE} := \varphi_i\big|_{\Omega_{\mathcal{T}_i}}$, where $(\varphi_i)_i$ denotes a basis of the space $V_h(\Omega_{\mathcal{T}_i})$.

For the assembly of the mass matrix $M_i = \left(\int_{\Omega_i} \varphi_i^{CFE} \varphi_j^{CFE} \,\mathrm{d}\mathbf{x}\right)_{ij}$ and stiffness matrix $L_i = \left(\int_{\Omega_i} \nabla\varphi_i^{CFE} \nabla\varphi_j^{CFE} \,\mathrm{d}\mathbf{x}\right)_{ij}$ we need to apply quadrature rules for functions on $T \cap \Omega_i$. On each cell T, which is crossed by the zero level-set of u we generate on-the-fly a partition of $T \cap \Omega_i$ into simplices and apply a barycenter quadrature rule on each simplex.

In order to apply a multigrid method, we generate a sequence of nested Composite Finite Element spaces by applying an approriate coarsening process on the CFE triangulation on the finest level $l_{\max}$ ($\Omega_{\mathcal{T}_i}^{l_{\max}} := \Omega_{\mathcal{T}_i}$), i. e.

$$\Omega_i \subset \Omega_{\mathcal{T}_i}^{l_{\max}} \subset \Omega_{\mathcal{T}_i}^{l_{\max}-1} \subset \ldots \subset \Omega_{\mathcal{T}_i}^{0} \tag{6.3}$$

leading to correspondingly nested CFE spaces $V_h^{CFE}(\Omega_{\mathcal{T}_i}^l)$, $0 \leq l \leq l_{\max}$. Prolongations and restrictions naturally have to be defined with respect to the CFE discretization, hence prolongation onto level l is defined by evaluation of the basis functions $\varphi_i^{CFE,l-1}$ for Lagrange nodes on level l. Convergence analysis for multigrid algorithms using Composite Finite Elements has been investigated by Sauter et al. [34, 61] and we refer to [33] for a comprehensive overview of geometric multigrid methods.

7. Numerical Experiments

We have tested our approach in different scenarios. Figure 2 shows an synthetic image pair, which was designed to test the method in cases, where only *very litte common information* is contained in the images. The rotated shape on the upper left is supposed to be fitted into the structure on the bottom left, which is hence only determined by the four small objects in the corners of the image. After 75

steps of the gradient descent, a deformation is found which rotates the propeller-like shape, and the resulting push-forward of the contour matches quite well to the rounded corners in the second structure in the bottom. Hence this example shows the capability of a model-based inpainting, where the shape information of the inpainted contour is transformed from a reference image. We assume, that the deviations from the obvious solution of a pure rotation result from the fact, that the rigid transformations are not in the kernel of our regularization energy, and we think that this could be improved by a different regularization method as for example a higher order method [47].

Figure 8 shows again the capability of the method to use complementary information from both images. In this situation, however, both images are contaminated by noise. As a by-product we also obtain smoothed reference and template images shown on the right-hand side of Figure 8 where the edges detected by the segmentation are preserved. This holds especially for the weak upper edge of the triangle in the second image.

In Figure 8 we have applied the algorithm to a pair of brain images. The top row shows a positron density (PD) scan, while the bottom row shows a T1-weighted magnetic resonance image of the same patient. The initial difference of the image pair consists mainly of a translation of about 8-9 pixels. The algorithm finds the brain structure in both images well after about 80 steps, and the resulting deformation consists mainly of a shift enhanced by some minor locally detailed deformations. This example underlines the practicability of the level-set approach: after a few steps the initial contour splits up into three different components which are henceforth indepently mapped onto the corresponding segments in the template.

The last example in Figure 8 demonstrates the competing effect of the regularization and the energy contributions which pull the contour towards the edges. We can exploit this in order to map an original reference shape (top row) to a given object, where the shape is partially corrupted (bottom row). Apart from the destroyed region the shapes differ also by a non-rigid deformation plus a translation. This can be well observed in the second column. Here the deformation is still close to the identity and hence the contours are aligning to the edges in the vicinity first until in subsequent iterations the deformation evolves in such a way that the contours map to the true edges in both images apart from the borders of destroyed region. At this stage, the regularization dominates and prohibits the contour in the bottom row to evolve towards the "visible" edge and prefers to adopt the contour from the reference image. This yields a reconstruction of the destroyed shape, which is optimal with respect to the regularization energy.

8. Discussion

We have presented a level-set based algorithm for simultaenous segmentation and registration of images by incorporating a Mumford-Shah type energy on the reference image as well as the template image, where the contour is transformed into the template image by a regularized deformation. The work presented here is motivated by the fact, that given an exact registration of two images of different modality, edge-extraction and segmentation can be enhanced considerably by combining complementary feature information from both modalities. On the other hand the process of registering a pair of images may rely on segmentations and feature-extractions of both images, which often is a very tedious process, especially if in some areas the feature information is very weak. Due to the coupling of the edge sets by the smooth deformation, the edge is in such areas driven to its correct shape.

We have demonstrated a further important application of this method, namely that this approach may also be used to perform a fully-automatic model-based reconstruction and inpainting of destroyed regions, without having to explicitly mark the region where the object is destroyed as long there are no prominently dominating edges. Although the results are already very promising, there is still room for further conceptual modelling, e. g., to avoid competition of the broken edge and the reference edge along the boundary of the destroyed region.

Due to the regularization of the gradient flow, the minimization process has turned out to be stable and requiring only a relativly small number of iterations until convergence. On the other hand, the regularization and necessity of determining the solutions of the Helmholtz equations in the regions Ω_1 and Ω_2. In order to make the method efficient we have applied multigrid techniques which lead to an enormous speed-up of the algorithm.

We have performed all calculations using only the first variations of the energy. In further studies, one might investigate Levenberg-Marquart (cf. [10]) or pure Newton-type methods to further accelerate the minimization process.

Acknowledgement

The authors would like to thank Martin Rumpf for many helpful comments and Florian Liehr for many advices concerning the Composite Finite Element method. Furthermore we want to thank Carlo Schaller for many stimulating discussion on medical imaging and computer aided surgery.

References

[1] L. Ambrosio, N. Fusco, and D. Pallara. *Functions of bounded variation and free discontinuity problems*. Oxford University Press, 2000.

[2] L. Ambrosio and V. M. Tortorelli. Approximation of functionals depending on jumps by elliptic functionals via Γ-convergence. *Comm. Pure Appl. Math.*, 43:999–1036, 1990.

[3] L. Ambrosio and V. M. Tortorelli. On the approximation of free discontinuity problems. *Boll. Un. Mat. Ital. B*, 6(7):105–123, 1992.

[4] Gilles Aubert and Pierre Kornprobst. *Mathematical problems in image processing*. Springer-Verlag, New York, 2002. Partial differential equations and the calculus of variations, With a foreword by Olivier Faugeras.

[5] J.M. Ball. Global invertibility of Sobolev functions and the interpenetration of matter. *Proc. Roy. Soc. Edinburgh*, 88A:315–328, 1988.

[6] A. Bonnet. On the regularity of the edge set of Mumford-Shah minimizers. *Prog. in Nonlinear Differential Equations and Their Applications*, 25:93–103, 1996.

[7] B. Bourdin and A. Chambolle. Implementation of an adaptive Finite-Element approximation of the Mumford-Shah functional. *Numer. Math.*, 85(4):609–646, 2000.

[8] A. Braides. *Approximation of Free Discontinuity Problems*, volume 1694 of *Lecture Notes in Mathematics*. Springer-Verlag, 1998.

[9] M. Burger. A framework for the construction of level set methods for shape optimization and reconstruction. *Interfaces and Free Boundaries*, 5:301–329, 2003.

[10] M. Burger. Levenberg-Marquardt level set methods for inverse obstacle problems. *Inverse Problems*, 20(1):259–282, 2004.

[11] M. Burger, B. Hackl, and W. Ring. Incorporating topological derivatives into level set methods. *J. Comp. Phys.*, 194(1):344–362, 2004.

[12] V. Caselles, F. Catté, T. Coll, and F. Dibos. A geometric model for active contours in image processing. *Numer. Math.*, 66:1–31, 1993.

[13] V. Caselles and B. Coll. Snakes in movement. *SIAM J. Numer. Anal.*, 33(6):2445–2456, 1996.

[14] V. Caselles, R. Kimmel, and G. Sapiro. Geodesic active contours. *International Journal of Computer Vision*, 22(1):61–79, 1997.

[15] A. Chambolle. Image segmentation by variatonal methods: Mumford-Shah functional and the discrete approximations. *SIAM J. Appl. Math.*, 55(3):827–863, 1995.

[16] T. F. Chan and L. A. Vese. Image segmentation using level sets and the piecewise constant Mumford-Shah model. UCLA CAM Report 00-14, University of California , Los Angeles, 2000.

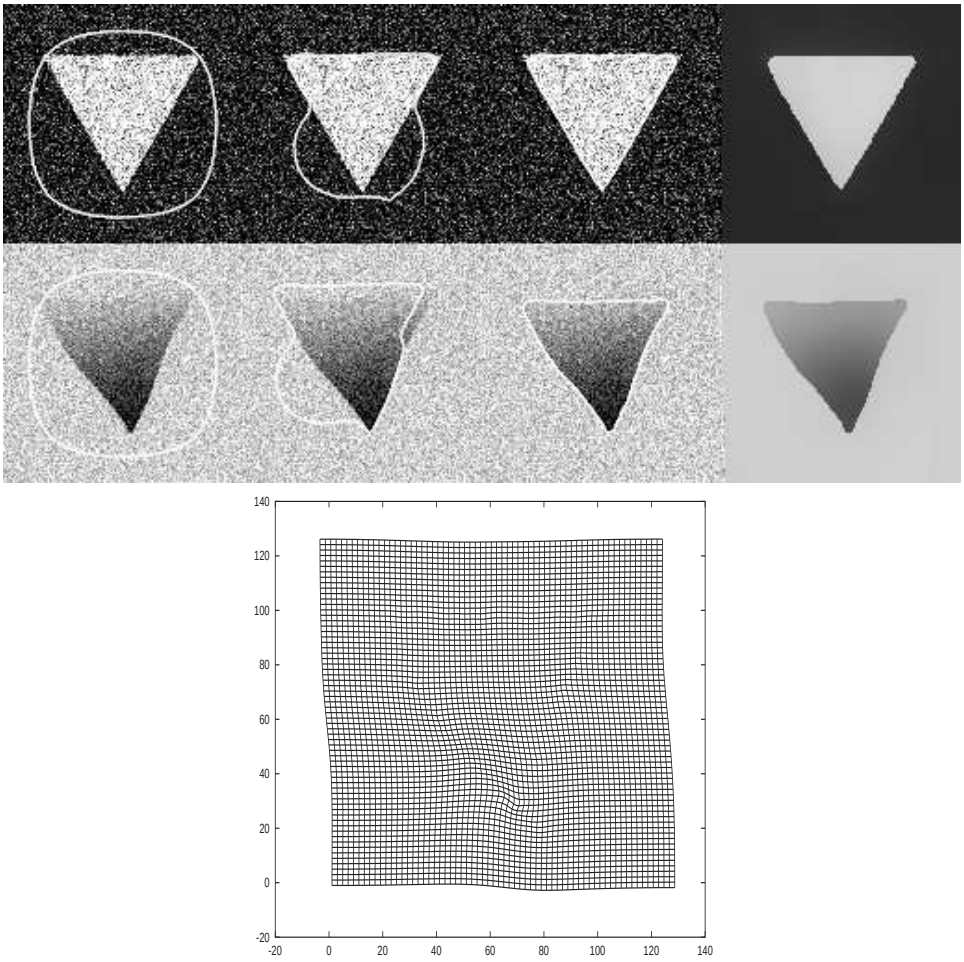

FIGURE 2. Simultaneous segmentation, registration, and denoising of two artificial test images. The smoothed reconstructions of both images are shown on the right hand side.

[17] T. F. Chan and L. A. Vese. A level set algorithm for minimizing the Mumford-Shah functional in image processing. UCLA CAM Report 00-13, University of California , Los Angeles, 2000.

[18] T. F. Chan and L. A. Vese. Active contours without edges. *IEEE Trans. Image Processing*, 10(2):266–277, 2001.

[19] Ph. G. Ciarlet. *The finite element method for elliptic problems*. North Holland, Amsterdam, 1978.

[20] Philippe G. Ciarlet. *Mathematical elasticity. Vol. I*, volume 20 of *Studies in Mathematics and its Applications*. North-Holland Publishing Co., Amsterdam, 1988. Three-dimensional elasticity.

[21] U. Clarenz, M. Droske, and M. Rumpf. Towards fast non–rigid registration. In *Inverse Problems, Image Analysis and Medical Imaging, AMS Special Session Interaction of Inverse Problems and Image Analysis*, volume 313, pages 67–84. AMS, 2002.

[22] U. Clarenz, S. Henn, and K. Rumpf, M. Witsch. Relations between optimization and gradient flow methods with applications to image registration. In *Proceedings of the 18th GAMM Seminar Leipzig on Multigrid and Related Methods for Optimisation Problems*, pages 11–30, 2002.

[23] D. Cremers, T. Kohlberger, and C. Schnörr. Nonlinear shape statistics in mumford-shah based segmentation. In A. Heyden et al., editor, *7th European Conference on Computer Vision, Copenhagen, Springer LNCS*, volume 2351, pages 93–108, 2002.

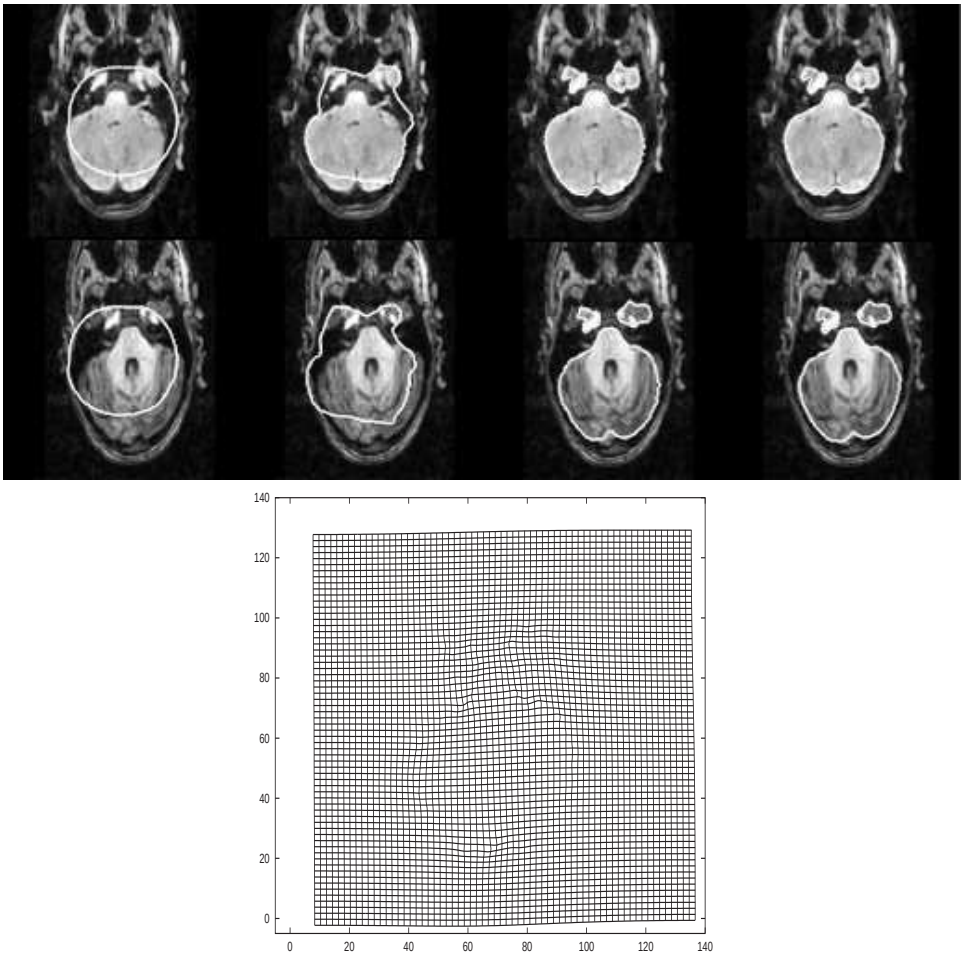

FIGURE 3. TOP ROW: Reference image R (positron density image (PD) of a human brain) and Γ. BOTTOM ROW: Template image T (T1-weighted MR image). The sequence shows the gradient descent for the iteration numbers $0, 10, 80$ and 180. The parameters were chosen as $\mu = 50$, $\alpha = 20$, $\nu = 500$. Images from the MPI of cognitive neurosciences, Leipzig.

[24] D. Cremers, F. Tischhäuser, J. Weickert, and C. Schnörr. Diffusion snakes: Introducing statistical shape knowledge into the mumford-shah functional. *International Journal of Computer Vision*, 50(3):1364–1379, 2002.

[25] G. Dal Maso, J.M. Morel, and S. Solimini. A variational method in image segmentation: existence and approximation results. *Acta Math.*, 168(1-2):89–151, 1996.

[26] C. A. Davatzikos, R. N. Bryan, and J. L. Prince. Image registration based on boundary mapping. *IEEE Trans. Medical Imaging*, 15(1):112–115, 1996.

[27] E. De Giorgi, M. Carriero, and A. Leaci. Existence theorem for a minimum problem with free discontinuity set. *Arch. Rat. Mech. and Anal.*, 108:195–218, 1989.

[28] M. C. Delfour and J.-P. Zolésio. *Shapes and geometries*. Society for Industrial and Applied Mathematics (SIAM), Philadelphia, PA, 2001. Analysis, differential calculus, and optimization.

[29] M. Droske and M. Rumpf. A variational approach to non-rigid morphological registration. *SIAM Appl. Math.*, 64(2):668–687, 2004.

[30] S. Esedoglu and S. Jianhong. Digital inpainting based on the mumford-shah-euler image model. *Euro. Jnl. Appl. Math.*, 2002.

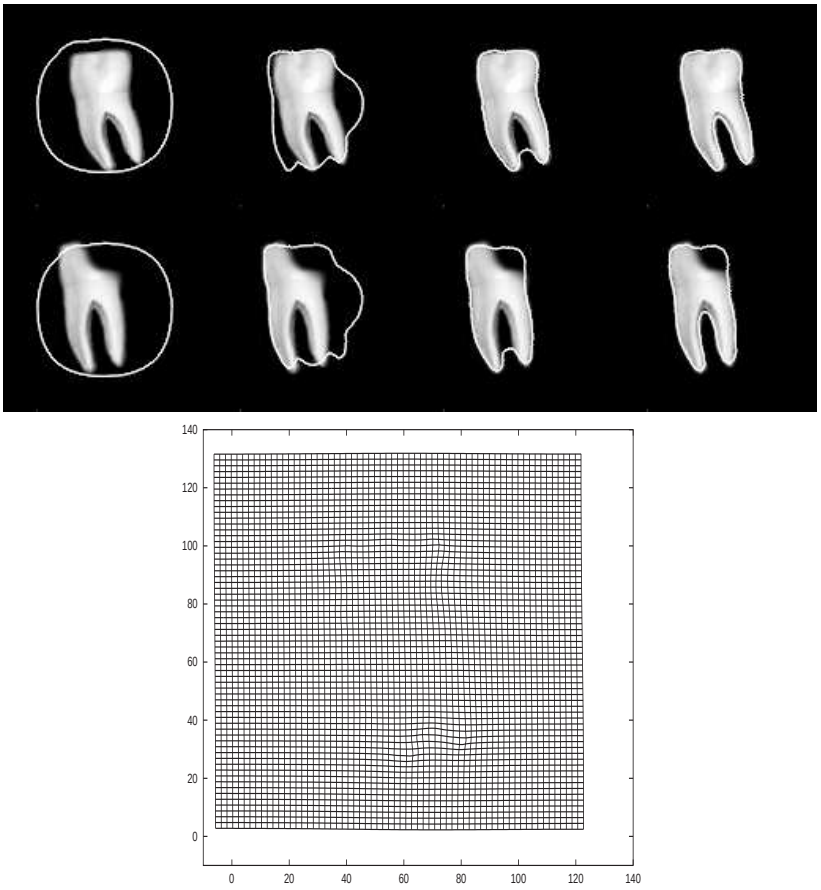

FIGURE 4. Matching a reference to a template with a destroyed region. The image in the bottom row also differs non-rigidly from the image in the top row. The edge set of the reference is matched onto the contours of the template, where it does not contradict strongly to the regularity of the deformation. The parameters were chosen as $\mu = 50$, $\alpha = 200$ and $\nu = 5000$. The bottom image shows the deformation plot.

[31] L. C. Evans and R. F. Gariepy. *Measure Theory and Fine Properties of Functions*. CRC Press, 1992.
[32] X. Feng and A. Prohl. Analysis of gradient flow of a regularized Mumford-Shah functional for image segmentation and image inpainting. *Mathematical Modelling and Numerical Analysis*, 38(2):291–320, 1999.
[33] W. Hackbusch. *Multigrid Methods and Applications*. Springer, Berlin/Heidelberg, 1985.
[34] W. Hackbusch and S. Sauter. Composite finite elements for the approximation of pdes on domains with complicated micro-structures. *Numerische Mathematik*, 75:447–472, 1997.
[35] S. Henn. A Levenberg-Marquardt scheme for nonlinear image registration. *BIT Numerical Mathematics*, 43(4):743–759, 2003.
[36] S. Henn and K. Witsch. A multigrid approach for minimizing a nonlinear functional for digital image matching. *Computing*, 64(4):339–348, 2000.
[37] M. Hintermüller and W. Ring. An inexact Newton-CG-type active contour approach for the minimization of the Mumford-Shah functional. *J. Math. Imag. Vis.*, 20(1–2):19–42, 2004.
[38] B.K.P. Horn and B.G. Schunk. Determining optical flow. *Artificial Intelligence*, 17:185–204, 1981.
[39] S. C. Joshi and M. I. Miller. Landmark matching via large deformation diffeomorphisms. *IEEE Transactions on Image Processing*, 9(8):1357–1370, 2000.

[40] T. Kapur, L. Yezzi, and L. Zöllei. A variational framework for joint segmentation and registration. *IEEE CVPR - MMBIA*, pages 44–51, 2001.
[41] M. Kass, A. Witkin, and D. Terzopoulos. Snakes: Active contour models. *International Journal of Computer Vision*, 1(4):321–331, 1988.
[42] S. L. Keeling and W. Ring. Medical image registration and interpolation by optical flow with maximal rigidity. *J. Math. Imag. Vis.*, 2005.
[43] A Kirsch. *An Introduction to the Mathematical Theory of Inverse Problems*, volume 120 of *applied mathematical sciences*. Springer Verlag, New York, 1996.
[44] F. Maes, A. Collignon, D. Vandermeulen, G. Marchal, and P. Suetens. Multi–modal volume registration by maximization of mutual information. *IEEE Trans. Medical Imaging*, 16, no. 7:187–198, 1997.
[45] R. Malladi, J. A. Sethian, and B. C. Vemuri. Shape modeling with front propagation: A level set approach. *IEEE Transactions on Pattern Analysis and Machine Intelligence*, 17(2):158–175, 1995.
[46] M.I. Miller, A. Trouvé, and L. Younes. On the metrics and euler-lagrange equations of computational anatomy. *Annual Review of Biomedical Enginieering*, 4:375–405, 2002.
[47] J. Modersitzki and B. Fischer. Curvature based image registration. *JMIV*, 18(1), 2003.
[48] P. Monasse. Contrast invariant registration of images. In *Proceedings of the International Conference on Acoustics, Speech and Signal Processing, Phoenix, Arizona*, volume 6, pages 3221–3224, 1999.
[49] J.M. Morel and S. Solimini. *Variational models in image segmentation*. Birkäuser, 1994.
[50] D. Mumford and J. Shah. Optimal approximation by piecewise smooth functions and associated variational problems. *Comm. Pure Appl. Math.*, 42:577–685, 1989.
[51] H. H. Nagel and W. Enkelmann. An investigation of smoothness constraints for the estimation of displacement vector fields from image sequences. *IEEE Trans. Pattern Anal. Mach. Intell.*, 8(5):565–593, 1986.
[52] S. J. Osher and R. P. Fedkiw. *Level Set Methods and Dynamic Implicit Surfaces*. Springer-Verlag, 2002.
[53] S. J. Osher and N. Paragios. *Geometric Level Set Methods in Imaging, Vision and Graphics*. Springer, 2003.
[54] S. J. Osher and J. A. Sethian. Fronts propagating with curvature dependent speed: Algorithms based on Hamilton–Jacobi formulations. *J. of Comp. Physics*, 79:12–49, 1988.
[55] T. J. Richardson and S. K. Mitter. A variational formulation based edge focussing algorithm. *Sadhana Acad. P. Eng. S.*, 22(4):553–574, 1997.
[56] S. Sauter and N. Stahn. Composite finite elements and multi-grid. part i: Convergence theory in 1-d. Technical Report Preprint, 11-01, University of Zürich, 2001.
[57] J. A. Sethian. *Level Set Methods: Evolving Interfaces in Geometry, Fluid Mechanics, Computer Vision and Materials Sciences*. Cambridge Univ. Press, 1996.
[58] J. Sokołowski and J-P. Zolésio. *Introduction to shape optimization*. Springer-Verlag, Berlin, 1992. Shape sensitivity analysis.
[59] A. Tsai, A. Yezzi, and A. Willsky. Curve evolution implementation of the Mumford-Shah functional for image segmentation, denoising, interpolation, and magnification. *IEEE Transactions on Image Processing*, 10(8):1169–1186, 2001.
[60] B.C. Vemuri, J. Ye, Y. Chen, and C.M. Leonard. Image registration via level-set motion: Applications to atlas-based segmentation. *Medical Image Analysis*, 7:1–20, 2003.
[61] R. Warnke. Schnelle löser für elliptische randwertprobleme mit springenden koeffizienten. *Dissertation, Zürich*, 2003.
[62] W. Wells, P. Viola, H. Atsumi, S. Nakajima, and R. Kikinis. Multi-modal volume registration by maximization of mutual information, 1996.

Department of Mathematics, University of California, 520 Portola Plaza, Los Angeles, CA, 90055
E-mail address: droske@math.ucla.edu

♯Special Research Center on Optimization and Control, Institute of Mathematics, University of Graz, Heinrichstrasse 36, A-8010 Graz, Austria.
E-mail address: wolfgang.ring@uni-graz.at